# Through-the-Wall Multi-Person Localization using Translation and Rotation Synthetic Aperture Radar

S. Sinha\*, A. Deshwal\*, A. Azizi<sup>†</sup>, D. Pandey<sup>†</sup>, N. Mehrotra<sup>†</sup>, A. Pal\*, A. Sabharwal<sup>†</sup>

\*Indian Institute of Technology Kanpur, Uttar Pradesh, India

<sup>†</sup>Rice University, Houston, Texas, United States

Abstract—An emerging application of wireless sensing is locating and tracking humans in their living environments, a primitive that can be leveraged in both daily life applications and emergency situations. However, most proposed methods have limited spatial resolution when multiple humans are in close vicinity. The problem becomes exacerbated when there is no lineof-sight path to the humans. In this paper, we consider multiperson localization of humans in close vicinity of each other. We propose the use of synthetic aperture radar that combines both translation and rotation to increase effective aperture size, leveraging small rhythmic changes in the radar range due to human breathing. We experimentally evaluate the proposed algorithm in both line-of-sight and through-wall cases with three to five humans in the scene. Our experimental results show that: (i) larger synthetic apertures due to radar translation improve multi-person localization, e.g., by  $1.42\times$  when the aperture size is increased by a factor of  $2\times$ , and (ii) rotation can largely compensate for gains provided by translation, e.g., rotating the radar over 360° without changing the aperture size results in  $1.22\times$  gains over no rotation. Overall, maximal gains of  $2.19\times$  are achieved by rotating and translating over a  $2\times$  larger aperture.

Index Terms—Multi-Person Localization, Synthetic Aperture Radar, UWB Radar, Translation and Rotation Radar.

### I. Introduction

The increasing demand for precise, non-invasive localization of human targets in through-the-wall (TTW) scenarios has attracted considerable research interest over the past decade [1]–[3]. Such TTW human localization has a wide range of applications, such as smart homes, security systems, emergency response, disaster management etc. Traditional localization methods, such as cameras or wearable devices, often suffer from privacy concerns, occlusions, and the need for continuous human interaction or are infeasible in constrained environments with low visibility, such as a disaster site. Hence, WiFi-based or Ultra-wideband (UWB) radar-based solutions are often considered for human vital sign detection.

**Prior Literature:** Given the near-ubiquity of WiFi infrastructure, WiFi-based solutions offer a cost-effective and readily deployable option for several indoor sensing use cases [4]–[7]. However, most WiFi signals have low bandwidth compared to UWB radar, resulting in reduced angular resolution for distinguishing closely spaced targets in cluttered and congested environments. UWB Radar signals, in contrast, can penetrate obstacles, operate in low-visibility conditions, and have higher

This research was supported by the IIT Kanpur Initiation Grant IITK/CS/2021164, IITK-Rice University Strategic Collaboration Award IITK/DOIR/2023227, and NSF Grants 1956297 and 2215082

bandwidths, providing better resolution and making it more suitable for detecting multiple individuals in closed spaces.

Several systems employ UWB radar for vital sign detection. such as Multi-Breath [8], which employs image processing techniques and tracks respiration in multiple individuals. Similarly, algorithms like Harmonic Multiple Loop Detection (HMLD) [9] improve heart and respiration rate estimation through cyclic spectrum updates. Deep learning techniques, such as ResNet [10] and MoVi-Fi [11] have been proposed to improve accuracy in detecting vital signs even under significant motion. Higher-order harmonics peak selection has been proposed in [12] for heart rate and respiration rate. However, most of these methods consider only line-of-sight targets. For behind-the-wall person detection, variable mode decomposition (VMD) has been used to extract breathing signals from UWB radar captures in [13], [14]. The use of UWB radar for simultaneously reconstructing obstacle layouts and localizing human targets behind them has been considered in [15], [16]. Authors in [17]-[24] have studied synthetic aperture radar (SAR) for target detections in non-line-of-sight environments. While promising, these techniques have been proposed and evaluated for a limited number of human targets. Thus multi-person localization using UWB radar remains a topic of interest to be explored in detail.

Contributions: In this paper, we propose a novel approach involving translation and rotation SAR to improve the detection and localization of closely spaced human targets. By placing the radar at multiple strategic positions and also rotating it on its axis at each location, we create a multiview synthetic aperture that enhances target resolution. Our proposed algorithm combines these radar captures from all radar locations and orientations. We use peak detection and grouping to create intensity maps of the scene that can be filtered and analyzed to detect multiple human targets. We experimentally evaluate the proposed heuristic with different numbers of human targets in various line-of-sight (LoS) and TTW settings. Through our experiments, we demonstrate that 2× larger synthetic apertures due to translation improve multiperson localization error by  $1.42\times$ . Furthermore, we show that rotation can be used to effectively compensate for any lack of translation freedom, and best performance of  $2.19 \times$  is achieved by rotating and translating over  $2 \times$  larger apertures.

One of our inspirations for exploring multi-person localization is rescuing humans during emergencies from cluttered environments. Radars could be mounted on the helmets of

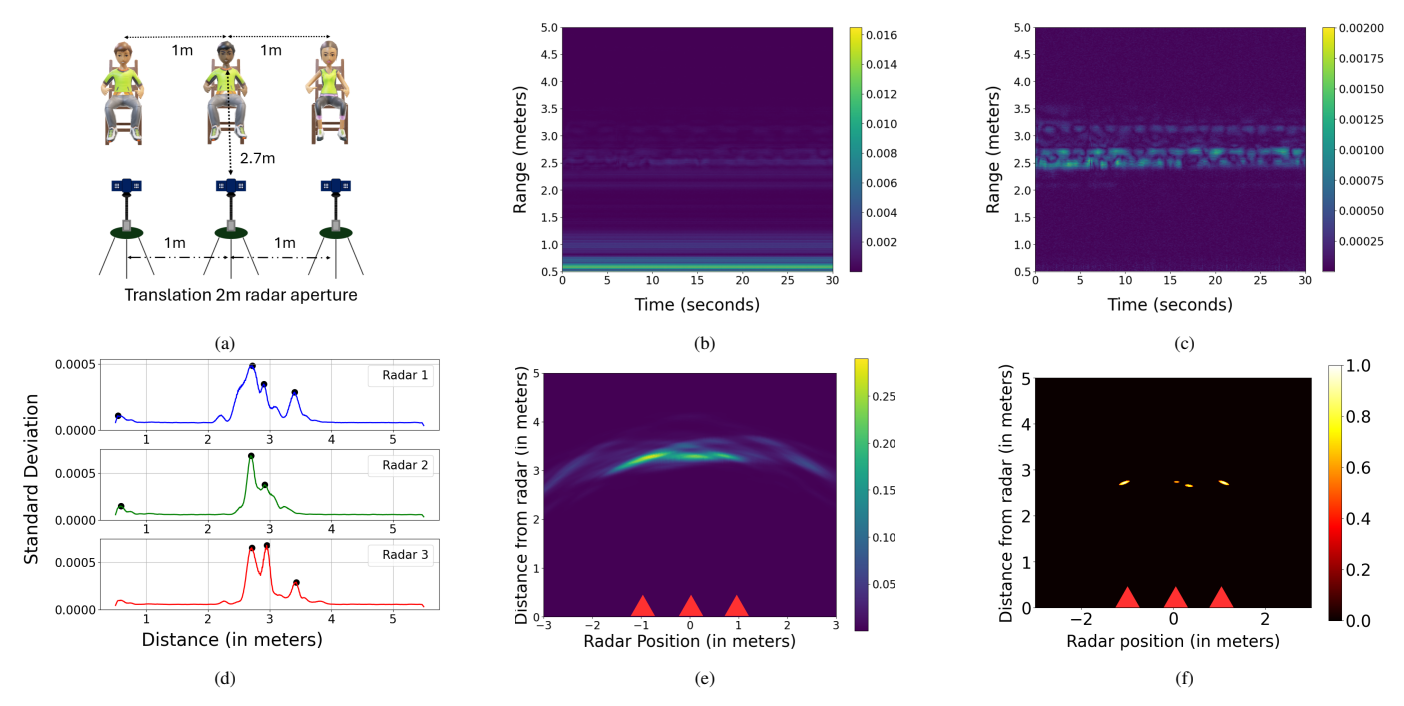


Fig. 1: (a) Illustration of our toy experimental setup, along with the (b) raw echo matrix  $M_{\mathbf{p},s}$  from one of the radar positions. After removing the echos generated from the static surrounding, the (c) resultant matrix captures the effects of echos due to dynamic components. To find out the target range bins of our interest, we compute (d) the standard deviation  $\sigma_{\mathbf{p},s}$  of the dynamic components in each bin. (e) Simple superimposition of  $\sigma_{\mathbf{p},s}$  from all the radar positions do not clearly reveal the person's locations, however, superposition of our proposed intensity maps  $I_{\mathbf{p}}$  from each radar position gives (f) a clearer picture of the person's locations. In (e), (f),  $\blacktriangle$  denotes the radar positions.

rescue workers, and as they walk (translation) and look around (rotation), a larger effective aperture can be formed. Multiple radar recordings from several positions and orientations could be combined to not only expand the radar's effective field of view but also increase its spatial resolution [25]–[28].

# II. PROBLEM FORMULATION

We consider a system configuration with the radar placed at different positions  $\mathbf{p} \in \mathcal{P}$  and oriented at angles  $\theta_s = s\Delta\theta, s \in \{1,\cdots,S=\frac{360^\circ}{\Delta\theta}\}$  for rotation increment  $\Delta\theta^\circ.$  The radar transmits Gaussian pulses  $s(t_f) = \exp(\frac{-t_f^2}{2\sigma^2})$  across fast time  $t_f$  and receives delayed attenuated copies of the transmitted pulse due to objects in the environment. Multiple copies of the Gaussian pulse are transmitted across a slow time index  $t_s$ . We assume K human targets in the radar's field-ofview, whose 2D locations are  $\left\{\mathbf{x}_k(t_s) = \mathbf{x}_k + \Delta_k(t_s)\right\}_{k=1}^K$ , where  $\Delta_k(t_s)$  indicates slight variation in the 2D locations as a function of the slow time index  $t_s$  due to breathing-related chest movements. Then, the radar's measurements after matched filtering with the transmitted pulse can be written as:

$$r_{\mathbf{p},s}^{\mathsf{mf}}(t_f;t_s) = \sum_{k=1}^{K} \sqrt{\pi} \sigma \alpha_{k,s} e^{-\left(\frac{t_f - \frac{2\|\mathbf{x}_k(t_s) - \mathbf{p}\|_2}{c}}{2\sigma}\right)^2} + n_{\mathbf{p},s}, \quad (1)$$

where  $\alpha_{k,s}$  denotes attenuation for the  $k^{\text{th}}$  human when the radar transmits towards direction  $\theta_s$ , and  $n_{\mathbf{p},s}$  denotes noise due to multipath and surrounding secondary static objects.

Collecting the radar measurements across  $N_r$  fast time samples (or "range bins") and  $N_f$  slow time samples, we

obtain a  $N_r \times N_f$  2D radar echo matrix  $M_{\mathbf{p},s}$ . The goal is to estimate the locations  $\mathbf{x}_k$  of the humans from matrix  $M_{\mathbf{p},s}$ .

# III. PROPOSED ALGORITHM

The proposed algorithm consists of multiple stages – the initial step involves basic preprocessing techniques such as background subtraction to remove the echoes from the surrounding static objects. Subsequently, the dynamic signal components are extracted to detect motion, followed by combining the observation from multiple radar positions to identify the location of the individuals. The steps are summarized in the MPL Algorithm, which are illustrated as follows.

Extracting the breathing signals: The first step is to extract the breathing signals from  $M_{\mathbf{p},s}$ , which are often mixed with clutter interference. This is because the transmitted signal from a radar is reflected from the surrounding static environment, and therefore extracting the reflections from the human's body remains quite challenging. Fig. 1(b) shows the reflected signal from a typical UWB radar corresponding to a toy experimental scenario of Fig.1(a), which shows the effect of multiple reflected components. Therefore, we need to distinguish the components that are coming from the human's body from the ones that are reflected back from the static surroundings. To resolve this, we implement a "background subtraction" solution that extracts only the dynamic components, by subtracting the mean amplitude of the signals at different distances. This is expressed in equation (2), where  $\frac{1}{N_f} \sum_{j=1}^{N_f} M_{\mathbf{p},s}(i,j)$  captures the effects of the static surroundings, and  $\tilde{M}_{\mathbf{p},s}(i,j)$  is the resultant matrix after removing the echos due to neighboring

### Algorithm: Multi-Person Localization (MPL)

**Input:** Radar positions  $\mathcal{P}$ , number of rotation steps S, number of range bins  $N_r$ , number of slow-time frames  $N_f$ , Data matrix of size  $N_r \times N_f$  for each radar position and rotation  $M_{\mathbf{p},s}$ , window length for peak detection w, minimum number of radar position subsets  $n_p$ , threshold for filtering intensity maps  $\tau_I$ , intensity sharpness criteria  $\sigma_I$ 

**Output:** Set of estimated 2D locations of persons  $\{\hat{\mathbf{x}}_k\}$ 

1: Background subtraction:

$$\tilde{M}_{\mathbf{p},s}(i,j) = M_{\mathbf{p},s}(i,j) - \frac{1}{N_f} \sum_{j=1}^{N_f} M_{\mathbf{p},s}(i,j)$$
 (2)

2: Compute the standard deviation along the rows of  $\tilde{M}_{\mathbf{p},s}$ :

$$\sigma_{\mathbf{p},s}(i) = \sqrt{\frac{1}{N_f - 1} \sum_{j=1}^{N_f} \tilde{M}_{\mathbf{p},s}^2(i,j)}$$
(3)

3: Peak detection and grouping:

$$\begin{split} \forall \mathbf{p}, s: \quad \mathsf{PeakSet}(\mathbf{p}, s) &= \{d | \sigma_{\mathbf{p}, s}(d) \geq \sigma_{\mathbf{p}, s}(l) \\ &\quad l = d - w, \dots, d + w\} \end{split} \tag{4}$$

$$\forall \mathbf{p} \in \mathcal{P}: \quad \mathsf{Range}(\mathbf{p}) = \bigg\{ \bigcup_{s=1}^{S} \mathsf{PeakSet}(\mathbf{p}, s) \bigg\} \tag{5}$$

4: Form intensity map for given radar position p

$$I_{\mathbf{p}}(x) = \sum_{r \in \mathsf{Range}(\mathbf{p})} \frac{1}{\sqrt{2\pi\sigma_I^2}} \exp\left(-\frac{(\|\mathbf{x} - \mathbf{p}\|_2 - r)^2}{2\sigma_I^2}\right) \quad (6)$$

5: Combine intensity maps across different subsets of radar positions  $C_p = \{P_i | P_i \subseteq \mathcal{P}, |P_i| \geq n_p\}$  and perform multi-person localization:

$$\{\hat{\mathbf{x}}_k\} = \left\{ x | \sum_{P_i \in \mathcal{C}_p} \prod_{\mathbf{p} \in P_i} I_{\mathbf{p}}(x) \ge \tau_I \right\}$$
 (7)

static objects. Fig. 1(c) shows the background subtracted outcome of Fig. 1(b), which illustrates the presence of humans at distances of  $\sim$ 2-3 meters.

Finding the target range bins: The next step is to find out the probable bins where humans can be present. To achieve this, we compute the standard deviation  $\sigma_{\mathbf{p},s}$  of the dynamic components in each bin via equation (3). Fig. 1(d) shows the standard deviation of the received radar signals over time at different distances from the radar positions. This figure shows that the range bins having larger variations correspond to the bins where humans are present. Also, high variability is observed at several adjacent bins around the target distances where the humans are present.

**Location estimation:** The variability in radar signals can reveal the presence of people at different distances from the radar. To estimate the location of the people, we try two approaches. In the first approach, we superimpose the signal variations  $\sigma_{\mathbf{p},s}$  from multiple radar positions with an intuition that locations with larger signal variation imply the presence of people. The outcome of this approach is illustrated in Fig. 1(e), which shows some variations around 2-3 meters but cannot clearly reveal the location of the persons.

To alleviate this, we employ a peak finding algorithm to identify the distances that show higher signal variation from Fig. 1(d) as expressed in (4)-(5). After this step, we get the





Fig. 2: Experimental setups, (a) the participants sat in direct line-of-sight of the radar, and (b) the participants and the radar were separated by a 25 cm thick brick wall.

set of possible distances Range( $\mathbf{p}$ ) where high variations are observed. We next generate the intensity maps  $I_{\mathbf{p}}$  around the radar position  $\mathbf{p}$  with all distances  $r \in \mathsf{Range}(\mathbf{p})$ , where the intensity is highest at r, and decreases around that distance following a Gaussian function with standard deviation  $\sigma_I$ , as expressed in (6).

Finally, to accurately determine the person's locations, we take the product of the intensity maps from multiple radar positions, which is expressed as  $\prod_{\mathbf{p}\in P_i} I_{\mathbf{p}}(x)$  in (7). The intersections of these maps suggests the potential locations of individuals. In our implementation, with  $|\mathcal{P}|$  radar positions, we use various combinations of these positions (from  $\binom{|\mathcal{P}|}{n_n}$ ) to  $\binom{|\mathcal{P}|}{|\mathcal{P}|}$ . Intensity maps from all these combinations are superimposed to obtain a cumulative intensity map, with an intuition that even if noise affects the data from certain radar positions, it is unlikely to occur consistently across all the positions. Finally, locations beyond the 99<sup>th</sup> percentile of the intensity values are extracted from the intensity map to remove the multipath effects, noise, or false peak identifications as expressed in (7), where  $\{\hat{\mathbf{x}}_k\}$  denotes the set of all possible human locations, and  $\tau_I$  denotes 99th percentile intensity. Fig. 1(f) shows the output of this last step, showing estimated human locations close to their ground-truth locations.

Notice that the parameter  $\sigma_I$  influences the localization outcome and is chosen empirically in our study. A higher value of  $\sigma_I$  broadens the intensity maps, leading to high miss detections, whereas a lower value results in narrow intensity maps and therefore increases false positive rates. For our experiments in section IV, we set  $\sigma_I = 0.05$ .

# IV. EXPERIMENTAL RESULTS

# A. Implementation & Methodology

**Implementation:** We implement the MPL Algorithm using XeThru X4M03 IR-UWB radars [29] from Novelda, which have a single on-chip transmitter and receiver and operate in the 6-8.5 GHz and 7.25-10.2 GHz frequency bands. The radar has an operating range of 9.9 m and a 65° beamwidth in azimuth and elevation. In our experiments, we configure the radar to transmit at a center frequency of 7.29 GHz, with a bandwidth of 1.5 GHz and a sampling rate of 23.328 GHz. **Data collection:** We collect radar reflections from the environ-

**Data collection:** We collect radar reflections from the environment across different 2D radar positions and orientations, with the radar manually translated and rotated at 30° increments.

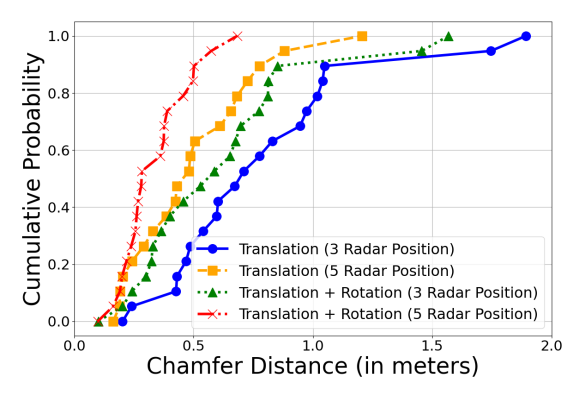


Fig. 3: Distribution of localization errors with translation and rotation SAR.

Fig. 1(a) illustrates an example scenario with 3 radar positions (spaced at 1 m increments) and 3 people in the environment. Data collection per radar position and orientation takes 30 s. **Experiment configurations:** We collect data in four key configurations: (1) translation-only, with the radar moved across three positions spaced at 2m and oriented towards  $0^{\circ}$ , (2) translation-only, with the radar moved across five positions spaced at 4m and oriented towards  $0^{\circ}$ , (3) translation + rotation, with the radar moved across three positions spaced at 2m and rotated in  $[0^{\circ}, 359^{\circ}]$  in steps of  $30^{\circ}$ , and (4) translation + rotation, with the radar moved across five positions spaced at 4m and rotated in  $[0^{\circ}, 359^{\circ}]$  in steps of  $30^{\circ}$ . In each configuration, we conduct experiments in LOS and TTW scenarios shown in Figs. 2(a)-(b). In total, we collect data across 20 different settings.

**Ground truth:** We establish the ground truth 2D positions of humans in the environment with respect to a global coordinate system using a measuring tape.

**Performance metric:** We quantify the multi-person localization performance of our algorithm using the Chamfer distance [30]–[34], defined as follows between two sets of 2D locations  $A = \{\mathbf{a}_i \in \mathbb{R}^2\}_{i=1}^n$  and  $B = \{\mathbf{b}_j \in \mathbb{R}^2\}_{j=1}^m$ :

$$d_{A,B} = \frac{1}{2n} \sum_{i=1}^{n} \min_{\mathbf{b}_{j} \in B} \|\mathbf{a}_{i} - \mathbf{b}_{j}\|_{2} + \frac{1}{2m} \sum_{j=1}^{m} \min_{\mathbf{a}_{i} \in A} \|\mathbf{a}_{i} - \mathbf{b}_{j}\|_{2}.$$
(8)

In our evaluation,  $A = \{\mathbf{x}_k\}_{k=1}^K$  and  $B = \{\hat{\mathbf{x}}_k\}$  correspond to the sets of ground-truth and estimated 2D locations of the humans in the experimental setup. A lower Chamfer distance indicates better multi-person localization performance, with a Chamfer distance of zero indicating perfect localization.

### B. Results

Fig. 3 shows the cumulative distribution function (CDF) of the multi-person localization error of the MPL Algorithm, quantified via (8), over all 20 settings in which data was collected. We make two key observations from Fig. 3.

**Observation 1:** Larger synthetic apertures due to radar translation improve multi-person localization performance. Fig. 3 shows that 90th-percentile Chamfer distance improves by  $1.42\times$  when the radar is translated along a 4 m-long aperture (5 radar positions) vs a 2 m-long aperture (3 radar positions).

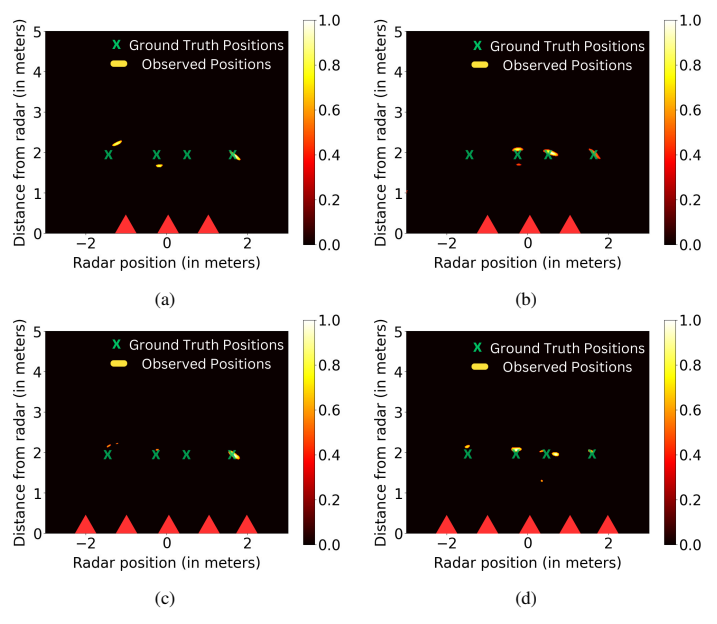


Fig. 4: Snapshots of location estimation results at different experimental instances, where the radar is translated along a 2m-long aperture (3 radar positions), (a) without and (b) with rotation. Larger synthetic apertures with 4m-long aperture (5 radar positions) (c) without and (d) with rotation, show improved localization performance. ▲ denotes the radar positions.

**Observation 2:** Rotation can compensate for gains provided by radar translation. Fig. 3 also shows that a large fraction of the gains achieved by translation along a 4 m-long aperture can be obtained instead by radar rotation even with a 2 m-long aperture. Specifically, the 90th-percentile Chamfer distance improves by  $1.22\times$  when the radar is rotated in  $[0^{\circ},359^{\circ}]$  with a 2 m-long aperture (3 radar positions) as compared to no rotation, which is comparable to the  $1.42\times$  gain achieved by radar translation along 4 m (5 radar positions). Moreover, the best performance  $(2.19\times$  gain) is achieved when the radar is translated and rotated along a 4 m-long aperture (5 positions) as compared to the radar translation along a 2 m-long aperture.

Figs. 4(a)-(d) show qualitative intensity plots corresponding to the four experimental configurations considered, with Fig. 4(a) corresponding to translation along a 2 m-long aperture (3 positions). The reconstruction improves with similar results when the radar is either: (i) rotated in  $[0^{\circ}, 359^{\circ}]$  without changing the aperture size in Fig. 4(b), or (ii) translated along a 4 m aperture (5 positions) in Fig. 4(c), thus verifying Observations 1 & 2. Finally, Fig. 4(d) shows the best qualitative performance when the radar is translated and rotated along a 4 m aperture (5 radar positions).

# V. Conclusion

This paper proposed leveraging radar translation and rotation to improve multi-person localization with UWB radars. We demonstrated proof-of-concept experimental results showing gains in localizing three to five people in 20 different line-of-sight and through-the-wall scenarios. Future work will generalize our proposed methodology to real-world deployments, e.g., in practical emergency operations with arbitrary radar trajectories and more cluttered environments.

### REFERENCES

- [1] Can Uysal and Tansu Filik, "A new RF sensing framework for human detection through the wall," *IEEE Trans. Veh. Tech.*, vol. 72, no. 3, pp. 3600–3610, 2022.
- [2] Binbin Xie, Minhao Cui, Deepak Ganesan, and Jie Xiong, "Wall Matters: Rethinking the Effect of Wall for Wireless Sensing," Proc. ACM Conf. Interactive, Mobile, Wearable Ubiquitous Techn., vol. 7, no. 4, pp. 1–22, 2024.
- [3] Fadel Adib, Chen-Yu Hsu, Hongzi Mao, Dina Katabi, and Frédo Durand, "Capturing the human figure through a wall," ACM Trans. Graphics, vol. 34, no. 6, pp. 1–13, 2015.
- [4] Xuyu Wang, Chao Yang, and Shiwen Mao, "PhaseBeat: Exploiting CSI Phase Data for Vital Sign Monitoring with Commodity WiFi Devices," in 2017 IEEE 37th Int. Conf. Dist. Comput. Sys. (ICDCS), 2017, pp. 1230–1239.
- [5] Jian Liu, Yan Wang, Yingying Chen, Jie Yang, Xu Chen, and Jerry Cheng, "Tracking Vital Signs During Sleep Leveraging Off-the-shelf WiFi," in *Proc. 16th ACM Int. Symp. Mobile Ad Hoc Netw. Comput.*, New York, NY, USA, 2015, MobiHoc '15, p. 267–276, Association for Computing Machinery.
- [6] Hongbo Sun, Lek Guan Chia, and Sirajudeen Gulam Razul, "Through-Wall Human Sensing With WiFi Passive Radar," *IEEE Trans. Aerosp. Electron. Syst.*, vol. 57, no. 4, pp. 2135–2148, 2021.
- [7] Xiang Zhang, Yu Gu, Huan Yan, Yantong Wang, Mianxiong Dong, Kaoru Ota, Fuji Ren, and Yusheng Ji, "Wital: A COTS WiFi devices based vital signs monitoring system using NLOS sensing model," *IEEE Trans. Human-Mach. Syst.*, vol. 53, no. 3, pp. 629–641, 2023.
- [8] Yanni Yang, Jiannong Cao, Xiulong Liu, and Xuefeng Liu, "Multi-Breath: Separate Respiration Monitoring for Multiple Persons with UWB Radar," in *IEEE 43rd Ann. Comput. Softw. App. Conf. (COMP-SAC)*, 2019, vol. 1, pp. 840–849.
- [9] Yi Zhang, Xiuping Li, Rui Qi, Zihang Qi, and Hua Zhu, "Harmonic Multiple Loop Detection (HMLD) Algorithm for Not-Contact Vital Sign Monitoring Based on Ultra-Wideband (UWB) Radar," *IEEE Access*, vol. 8, pp. 38786–38793, 2020.
- [10] Umer Saeed, Syed Yaseen Shah, Abdullah Alhumaidi Alotaibi, Turke Althobaiti, Naeem Ramzan, Qammer H. Abbasi, and Syed Aziz Shah, "Portable UWB RADAR Sensing System for Transforming Subtle Chest Movement Into Actionable Micro-Doppler Signatures to Extract Respiratory Rate Exploiting ResNet Algorithm," *IEEE Sensors J.*, vol. 21, no. 20, pp. 23518–23526, 2021.
- [11] Zhe Chen, Tianyue Zheng, Chao Cai, and Jun Luo, "MoVi-Fi: motion-robust vital signs waveform recovery via deep interpreted RF sensing," in *Proc.27th Ann. Int. Conf. Mobile Comput. Netw.*, New York, NY, USA, 2021, MobiCom '21, p. 392–405, Association for Computing Machinery.
- [12] Hongqiang Xu, Malikeh P. Ebrahim, Kareeb Hasan, Fatemeh Heydari, Paul Howley, and Mehmet Rasit Yuce, "Accurate Heart Rate and Respiration Rate Detection Based on a Higher-Order Harmonics Peak Selection Method Using Radar Non-Contact Sensors," Sensors, vol. 22, no. 1, 2022.
- [13] Huimin Yu, Wenjun Huang, and Baoqiang Du, "SSA-VMD for UWB Radar Sensor Vital Sign Extraction," Sensors, vol. 23, no. 2, 2023.
- [14] Aloysius Adya Pramudita, Ding-Bing Lin, Sung-Nien Hsieh, Erfansyah Ali, Harfan Hian Ryanu, Tjahjo Adiprabowo, and Ariana Tulus Purnomo, "Radar System for Detecting Respiration Vital Sign of Live Victim Behind the Wall," *IEEE Sensors J.*, vol. 22, no. 15, pp. 14670–14685, 2022.
- [15] Yongping Song, Jun Hu, Ning Chu, Tian Jin, Jianwen Zhang, and Zhimin Zhou, "Building Layout Reconstruction in Concealed Human Target Sensing via UWB MIMO Through-Wall Imaging Radar," *IEEE Geosci. Remote Sens. Lett.*, vol. 15, no. 8, pp. 1199–1203, 2018.
- [16] Amit Sarkar and Debalina Ghosh, "Accurate sensing of multiple humans buried under rubble using IR-UWB SISO radar during search and rescue," Sensors and Actuators A: Physical, vol. 348, pp. 113975, 2022.

- [17] Degui Yang, Zhengliang Zhu, Junchao Zhang, and Buge Liang, "The overview of human localization and vital sign signal measurement using handheld ir-uwb through-wall radar," Sensors, vol. 21, no. 2, 2021.
- [18] Risto Vehmas and Nadav Neuberger, "Inverse synthetic aperture radar imaging: A historical perspective and state-of-the-art survey," *IEEE Access*, vol. 9, pp. 113917–113943, 2021.
- [19] Maria Antonia Maisto, Mehdi Masoodi, Rocco Pierri, and Raffaele Solimene, "Sensor arrangement in through-the wall radar imaging," *IEEE Open Journal of Antennas and Propagation*, vol. 3, pp. 333–341, 2022.
- [20] Harikesh, Shakti Singh Chauhan, Ananjan Basu, Mahesh P. Abegaonkar, and Shiban Kishen Koul, "Through the wall human subject localization and respiration rate detection using multichannel doppler radar," *IEEE Sensors Journal*, vol. 21, no. 2, pp. 1510–1518, 2021.
- [21] Xiaqing Yang, Shihao Fan, Shisheng Guo, Songlin Li, Guolong Cui, and Wei Zhang, "Nlos target localization behind an 1-shaped corner with an 1-band uwb radar," *IEEE Access*, vol. 8, pp. 31270–31286, 2020.
- [22] Zhi Li, Tian Jin, Yongpeng Dai, and Yongkun Song, "Through-wall multi-subject localization and vital signs monitoring using uwb mimo imaging radar," *Remote Sensing*, vol. 13, no. 15, 2021.
- [23] Nishant Mehrotra, Divyanshu Pandey, Akarsh Prabhakara, Yawen Liu, Swarun Kumar, and Ashutosh Sabharwal, "Hydra: Exploiting Multi-Bounce Scattering for Beyond-Field-of-View mmWave Radar," in Proceedings of the 30th Annual International Conference on Mobile Computing and Networking, 2024, pp. 1545–1559.
- [24] Nishant Mehrotra, Divyanshu Pandey, Upamanyu Madhow, Yasamin Mostofi, and Ashutosh Sabharwal, "Instantaneous Velocity Vector Estimation Using a Single MIMO Radar Via Multi-Bounce Scattering," in 2024 IEEE Conference on Computational Imaging Using Synthetic Apertures (CISA), 2024, pp. 1–5.
- [25] Mojtaba Dehmollaian, Michael Thiel, and Kamal Sarabandi, "Throughthe-wall imaging using differential SAR," *IEEE Trans. Geosci. Remote Sens.*, vol. 47, no. 5, pp. 1289–1296, 2009.
- [26] Haowen Lai, Gaoxiang Luo, Yifei Liu, and Mingmin Zhao, "Enabling visual recognition at radio frequency," in *Proc. Annual Int. Conf. Mobile Comput. Netw.*, 2024, pp. 388–403.
- [27] Faiza Ali, Georg Bauer, and Martin Vossiek, "A rotating synthetic aperture radar imaging concept for robot navigation," *IEEE Trans. Microw. Th. Tech.*, vol. 62, no. 7, pp. 1545–1553, 2014.
- [28] Wei Zhao and Rong Zheng, "MARS: a mmWave Rotating Synthetic Aperture Radar System for Indoor Imaging," in Proc. ACM Workshop mmWave Sensing Syst. App., 2023, pp. 8–13.
- [29] Novelda AS, "Xethru x4m200 datasheet," 2019, Accessed: 2024-07-23.
- [30] Harry G Barrow, Jay M Tenenbaum, Robert C Bolles, and Helen C Wolf, "Parametric Correspondence and Chamfer Matching: Two New Techniques for Image Matching," in *Proc. Image Understanding Workshop*. Science Applications, Inc, 1977, pp. 21–27.
- [31] Zezhi Chen, Zsolt L Husz, Iain Wallace, and Andrew M Wallace, "Video Object Tracking Based on a Chamfer Distance Transform," in *IEEE Int.* Conf. Image Process., 2007, vol. 3, pp. III – 357–III – 360.
- [32] Tong Wu, Liang Pan, Junzhe Zhang, Tai WANG, Ziwei Liu, and Dahua Lin, "Balanced Chamfer Distance as a Comprehensive Metric for Point Cloud Completion," in *Advances in Neural Information Processing Systems*, M. Ranzato, A. Beygelzimer, Y. Dauphin, P.S. Liang, and J. Wortman Vaughan, Eds. 2021, vol. 34, pp. 29088–29100, Curran Associates, Inc.
- [33] Tomas Toss, Patrik Dämmert, Zoran Sjanic, and Fredrik Gustafsson, "Navigation with SAR and 3D-map aiding," in 18th Int. Conf. Info. Fusion, 2015, pp. 1505–1510.
- [34] Akarsh Prabhakara, Tao Jin, Arnav Das, Gantavya Bhatt, Lilly Kumari, Elahe Soltanaghai, Jeff Bilmes, Swarun Kumar, and Anthony Rowe, "High Resolution Point Clouds from mmWave Radar," in *IEEE Int. Conf. Robotics Automat. (ICRA)*, 2023, pp. 4135–4142.